Feasibility and clinical usefulness of modelling glioblastoma migration in adjuvant radiotherapy

Sven Knobe[a,*,1], Yvonne Dzierma[a,1], Michael Wenske[b], Christian Berdel[a], Jochen Fleckenstein[a], Patrick Melchior[a], Jan Palm[a], Frank G. Nuesken[a], Alexander Hunt[c], Christian Engwer[b], Christina Surulescu[d], Umut Yilmaz[e], Wolfgang Reith[e], Christian Rübe[a]

[a] Department of Radiotherapy and Radiation Oncology, Saarland University Medical Center, Homburg/Saar, Germany
[b] Institute for Analysis and Numerics, University of Muenster, Muenster, Germany
[c] Carl Zeiss Automated Inspection GmbH, Öhringen, Germany
[d] Felix Klein Centre for Mathematics, University of Kaiserslautern, Kaiserslautern, Germany
[e] Department of Diagnostic and Interventional Radiology, Saarland University Medical Center, Homburg/Saar, Germany

Received 17 December 2020; accepted 18 March 2021

Abstract

Glioblastoma (GBM) is one of the most common primary brain tumours in adults, with a dismal prognosis despite aggressive multimodality treatment by a combination of surgery and adjuvant radiochemotherapy. A detailed knowledge of the spreading of glioma cells in the brain might allow for more targeted escalated radiotherapy, aiming to reduce locoregional relapse. Recent years have seen the development of a large variety of mathematical modelling approaches to predict glioma migration.

The aim of this study is hence to evaluate the clinical applicability of a detailed micro- and meso-scale mathematical model in radiotherapy. First and foremost, a clinical workflow is established, in which the tumour is automatically segmented as input data and then followed in time mathematically based on the diffusion tensor imaging data. The influence of several free model parameters is individually evaluated, then the full model is retrospectively validated for a collective of 3 GBM patients treated at our institution by varying the most important model parameters to achieve optimum agreement with the tumour development during follow-up. Agreement of the model predictions with the real tumour growth as defined by manual contouring based on the follow-up MRI images is analyzed using the dice coefficient.

The tumour evolution over 103-212 days follow-up could be predicted by the model with a dice coefficient better than 60% for all three patients. In all cases, the final tumour volume was overestimated by the model by a factor between 1.05 and 1.47.

To evaluate the quality of the agreement between the model predictions and the ground truth, we must keep in mind that our gold standard relies on a single observer's (CB) manually-delineated tumour contours. We therefore decided to add a short validation of the stability and reliability of these contours by an inter-observer analysis including three other experienced radiation oncologists from our department. In total, a dice coefficient between 63% and 89% is achieved between the four different observers. Compared with this value, the model predictions (62-66%) perform reasonably well, given the fact that these tumour volumes were created based on the pre-operative segmentation and DTI.

Keywords: Bio-mathematical modelling, Glioblastoma growth and migration, Tumour segmentation, Inter observer analysis, Glioblastoma radiotherapy

* Corresponding author: S. Knobe, Universitätsklinikum des Saarlandes und Medizinische Fakultät der Universität des Saarlandes, Homburg, Germany.
E-mail: sven.knobe@uks.eu (S. Knobe).

[1] Joint first authors.

Z Med Phys **32** (2022) 149–158
https://doi.org/10.1016/j.zemedi.2021.03.004
www.elsevier.com/locate/zemedi

Introduction

Glioblastoma (GBM) is one of the most common primary brain tumours in adults, with a dismal prognosis despite aggressive multimodality treatment by a combination of surgery, adjuvant radiochemotherapy, and recent additions such as tumour-treating electromagnetic fields [1–4]. Over the past years, a joint endeavour by mathematicians, radiologists and biologists has been to understand the underlying mechanisms of tumour cell proliferation and invasion into the surrounding brain parenchyma by combining mathematical modelling approaches with cell investigations and imaging studies. As a result, a plethora of mathematical models have been developed which reflect the most fundamental biological properties of GBM, such as the go-or-grow dichotomy; themselves, these models have contributed to clarifying the necessity and possible biological bases of some of these properties [5–18].

With the evolving complexity of the models, the question arises whether the translation to the clinical treatment of glioblastoma patients can be achieved. This implementation is most promising for the field of radiotherapy, in such a way that predicting the spread of glioblastoma in the brain would enable more individualized target volume delineation and possible dose escalation so as to reduce tumour recurrences. However, to achieve this aim, reliable modelling predictions must be attainable in the realistic clinical setting, i.e., for patients with non-ideal data sets, with an adequate *a-priori* choice of model parameters.

The aim of this study is hence to evaluate the clinical applicability of a detailed micro- and meso-scale mathematical model [11] in radiotherapy. First and foremost, a clinical workflow is established. The model is then retrospectively validated for a collective of GBM patients treated at our institution. Practical issues such as the choice of input data, model parameters, and possible pitfalls are highlighted.

Although a few studies have evaluated different modelling approaches for radiotherapy [19–23], these have relied on relatively simplified modelling assumptions and placed their emphasis on radiotherapy target delineation or distant relapse patterns. In parallel, mathematical models continuously evolve towards higher complexity, which may bring them closer to the biological mechanisms, but not necessarily to the clinical reality. The aim of this study is not to present a sophisticated mathematical approach, but rather to take one step backwards and assess in how far a clinical implementation for an existing advanced model can be achieved and may realistically contribute to improved treatment of our patients.

Methods and materials

Biomathematical model

The underlying mathematical model is described by Engwer et al. [10–12]. In brief, this is a multi-scale mathematical approach including on the microscale subcellular dynamics of receptor binding, the interaction of glioma cells with anisotropic tissue on the mesoscale, and the evolution of the total tumour cell population on the macroscale. The most important underlying assumptions and model parameters are briefly outlined in the following.

We consider that tumour cells can perform the following actions: bind their receptors to ligands on tissue fibres or detach from the same, move at constant speed s, so that only the directions of their velocity vectors vary when the cells turn (instantaneously) with a rate depending on their receptor occupancies, move preferentially along fibre bundles, proliferate and die, naturally or under treatment. For each cell the number of receptors involved in such process (e.g., integrins) [24,25] is set constant as $R_0 = 10^5$ [26]. The detachment rate $k^- = 0.1\ \mathrm{s}^{-1}$ is taken from the literature [27], while the attachment rate k^+ is assumed to be of comparable magnitude, but remaining as a parameter to be optimized in the model. The effect of the tissue anisotropy on the cell orientation is modelled by a turning rate which involves a constant component $\lambda_0 = 0.8\ \mathrm{s}^{-1}$ [11] and a parameter λ_1 scaling the receptor occupancy variable; it is not *a-priori* known and included in the optimization of the model. In practice, λ_1 gives the sensitivity of the turning rate to changes in receptor occupancy. The migration speed of the cells is assumed to be constant, but allowed to vary within a reasonable parameter range, compatible with values available in the literature [28,29]. Cell proliferation is modelled as logistic, with growth rate $c_g = 8.44 \cdot 10^{-7}\ \mathrm{s}^{-1}$ [30]. The patient-specific DTI brain data is included in the model via the turning kernel involved in the reorientation operator on the mesoscopic level of description (for more details refer to [6–8,10–12,16]. The parabolic upscaling procedure therein leads to diffusion and drift terms containing in their coefficients the so-called tumour diffusion tensor encoding DTI information about the brain structure.

Workflow implementation and model adjustment

A major part of this work concerns the clinical implementation of the existing model into a practicable workflow, which is summarized in Figure 1. The most important steps are described here.

The initial tumour extension required as a model starting point is derived from the magnetic resonance images (MRI). As invasive cancer cells preferentially migrate along neuronal fibre tracts [12,25,31], these are estimated by diffusion tensor imaging (DTI) as additional model input. All data sets were retrieved retrospectively from the picture archiving and communication system (PACS) for all patients treated at our clinic between January 2012 and December 2016.

To ascertain a reproducible objective input dataset as starting point for the model, it was decided to use an automatic segmentation algorithm (BraTumIA), which combines the information from T1-weighted images with and without contrast media, T2-weighted and fluid-attenuated inversion

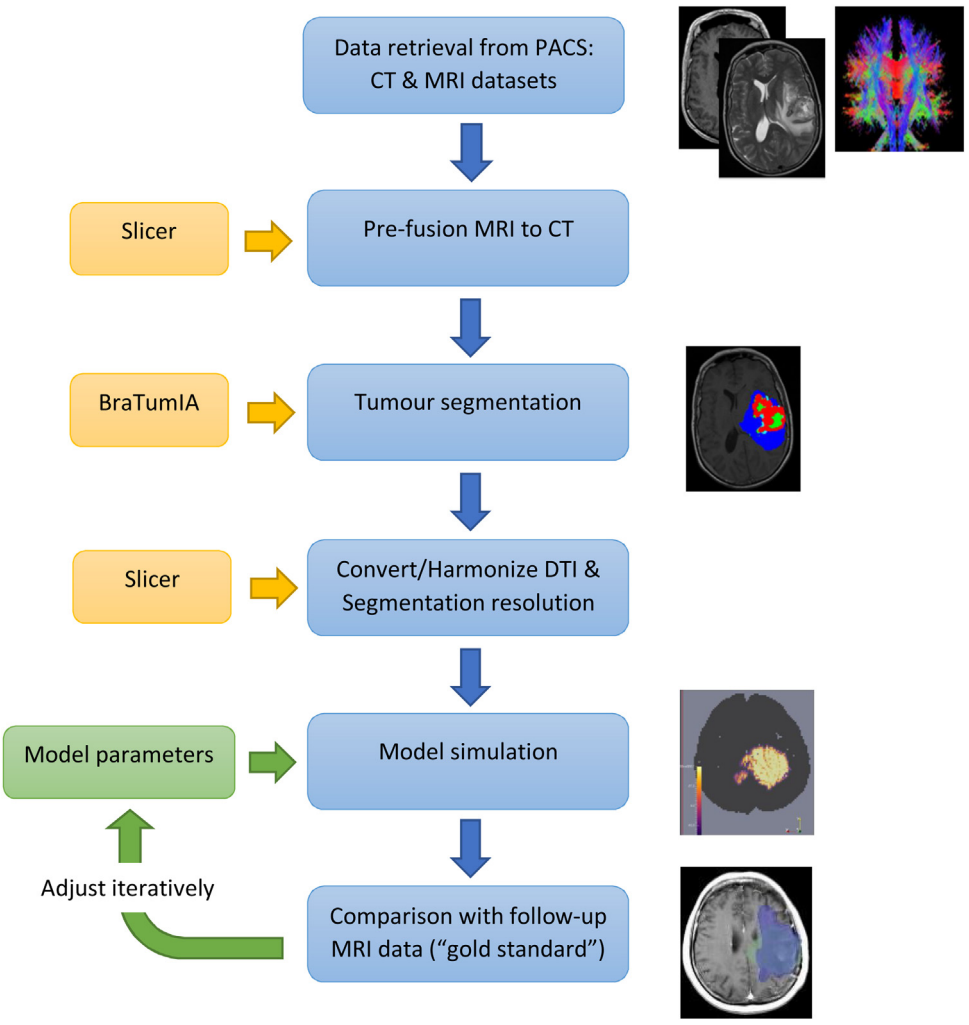

Figure 1. Main steps in implemented workflow to prepare data for tumour simulation and evaluation.

recovery (FLAIR) sequences [32]. The software automatically segments normal tissue, enhancing- and non-enhancing tumour, oedema, and necrosis. All segmentation results were validated visually against the "gold standard" as determined by an experienced radiation oncologist, with satisfactory results in agreement with the literature [33,34].

This software automatically co-registers datasets with different coordinate frames, and the output segmentation can be referenced to any desired data set – in our case, the DTI frame since this is the input for the mathematical modelling step. However, first experiences showed that sometimes the reference frames could not be adequately registered, so all data sets including the planning CT for further data processing in radiotherapy were rigidly co-registered in the Slicer3D software [35] before input into BraTumIA. This software was also used later in the workflow to convert structures into DICOM format (digital imaging and communication in medicine) before input in the treatment planning system (Philips Pinnacle V 16.2).

BraTumIA is designed for pre-operative images, and only for this time point was DTI information available. Therefore, tumour migration modelling needed to be started on the pre-operative segmentation and geometry. This may even be closer to the clinical reality since possibly, microscopic tumour invasion along white matter tracts will already have occurred by the time of macroscopic gross tumour resection. On the other hand, further migration will occur from the starting point of post-operative remaining tumour spread, so it was necessary to evaluate the influence of surgery on the tumour segmentation in a first step. This was done by comparing the segmentation volumes in the form of volume ratios and the dice coefficient DCC [36], which is defined for any two volumes X and Y as:

$$\mathrm{DCC} = 2 * |X \cap Y| / (|X| + |Y|)$$

At this point, all data sets were visually checked for plausibility before proceeding with the data processing and modelling. An in-house C++ code using the open source InsightToolkit-library (ITK) [37] transforms the DTI dataset

and segmentation to the same resolution. The DTI matrices are calculated from the DTI-data set using the Camino software [38]. With these input data sets, the model can be run with an appropriate choice of parameters. The numerical discretization was performed using the multipoint flux approximation method [39]. The model result is a three-dimensional representation of tumour cell densities in the patient's brain at a chosen time-point in the future.

To assess to which extent the model results corresponded to the real growth pattern of the tumour, the longest time point during follow-up for which MRI images were available was used for modelling. The model output was then compared with the tumour contour in the follow-up MRI images as determined by a senior radiation-oncologist (CB), hereafter referred to as "gold standard". Again, volume ratios and DCC were used for the comparisons.

Supplementary to the workflow implementation, the main part of this work consisted in finding the optimum parameters for realistic modelling results. This multi-parametric problem was approached step-wise as follows:

Firstly, the tumour cell densities in these tumour compartments (contrast media enhancing and nonenhancing tumour, necrosis and oedema) were adjusted within clinically realistic ranges. As in other modelling studies, it was expected that the tumour cell density within the volumes segmented as tumour (enhancing and non-enhancing) were between 80% and 100%. In fact, this choice had only little influence on the modelling results, so both tumour compartments were modelled with 100% cell density. Based on pathological information (Prof. Schulz-Schaeffer, personal communication), tumour cell densities in the oedema and necrosis volumes were assumed to fall between 0 and 20%. Within these ranges, several trial runs were performed with the extreme parameter values to assess the individual parameters' influence and obtain most plausible values. Comparing the model predictions for starting densities of 0% and 20% tumour cells in these compartments, it was found that a huge tumour volume encompassing nearly the complete brain resulted unless the tumour cell density in the oedema volume was set to 0, which was maintained for the following simulations. Most probably, this arises from the fact that BraTumIA is known to overestimate the amount of oedema [32], and tiny disseminated oedema islands within the brain parenchyma will coalesce over time in the modelling process. For the necrosis volume, 15% tumour cell density was presumed, which had only minor influence on the modelling results, being considerably smaller than the volume of viable tumour and contained therein.

Secondly, the influence of varying the cell migration speed s, receptor binding rate k^+ and constant λ_1 involved in the cell turning rate was examined by varying these parameters separately.

In the third and final step, an individual optimization of the parameters s and k^+ was carried out for each patient in a manual iterative approach starting by a coarse grid search followed by interval-nesting, and the quality of the best results was compared with the gold standard.

A final parameter entering into the model predictions is the level set with which the resulting tumour is displayed. The model output gives a map of predicted tumour cell densities, assigning each voxel a positive value since there is always a non-vanishing chance of finding tumour cells. To create a predicted tumour volume within the brain parenchyma, a threshold value must be chosen for which a voxel is considered to be either "tumour" or "normal tissue" – in a way, this is the converse of the initial input tumour cell density. In practice, this is similar to adjusting the window in CT images, so we refer to this parameter as "grey scale" or "level set". Within plausible values, this level set was also optimized for each patient, so as to remain consistent with the input methodology.

Patients

Initially, data for 44 patients was retrieved from the data base to be included in this analysis. However, a large number of patients needed to be excluded from the study either because insufficient initial imaging (6 patients) or follow-up MRI were available (13 patients), patients underwent more than one surgical intervention (4 patients), or survival was less than two months (6 patients). In further 12 cases (27% of patients), segmentation was impaired by artefacts for various reasons such as ventricular shunts, so that only 3 patient data sets remained for optimization. However, the intermediate steps in this analysis (such as comparison of pre- and post-operative segmentation results) did not require the complete data sets and larger patient collectives could be included, which will be detailed in the respective results.

Results

Comparison of segmentation results before and after surgery

For this analysis, all data sets were included for which pre- and post-operative MRI data were available for segmentation with less than a 7-day time interval, resulting in 10 patients (Table 1) with pre-operative tumour volumes ranging between 28.2 cm^3 and 251.9 cm^2. Pre- and post-operative tumour segmentations were performed alike by the BraTumIA software. In addition to the ratio of the segmented tumour volumes, the DCC is compared for the volume "normal brain", as the change in brain structure is relevant for the DTI consistency.

For all cases, the dice coefficients for the tumour-surrounding brain structure were larger than 80%, which is good agreement given the circumstances that a surgical procedure has taken place and the oedema volume is highly influenced by surgical and medical interventions. In 7 out of 10 patients, a tumour volume reduction is confirmed by segmentation, however, in the remaining 3 cases, the

Table 1
Differences between preoperative and postoperative tumour segmentation for patients with pre- and postoperative MR imaging less than 7 days apart.

Case #	Time interval pre-post [days]	Volume pre-OP [cm^3]	Volume post-OP [cm^3]	Ratio VpostOP/VpreOP	Dice coeff
1	0	116.385	124.257	1.07	0.84
2	0	251.922	225.015	0.89	0.83
3	1	28.197	46.242	1.64	0.95
4	1	48.558	70.920	1.46	0.89
5	1	134.784	125.712	0.93	0.89
6	1	125.073	123.561	0.99	0.81
7	1	226.461	187.722	0.83	0.88
8	3	115.122	100.686	0.87	0.91
9	4	140.796	115.668	0.82	0.82
10	4	68.493	63.960	0.93	0.93

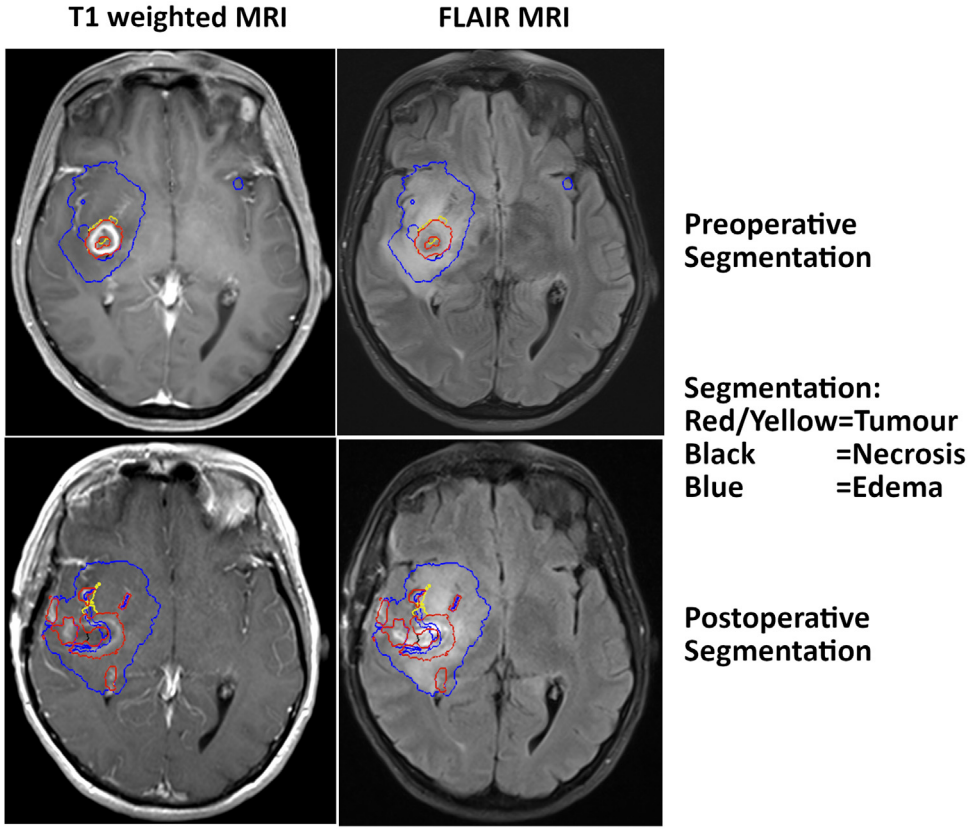

Figure 2. Preoperative and postoperative tumour segmentation for case #4. For this patient, postoperative bleeding into the resection cavity was falsely segmented as viable tumour. However, the oedema and brain volumes are correctly segmented. In general necrosis is segmented but actually not shown in the current slice.

segmented tumour volume after surgery is increased. To check this implausible result, these cases were individually scrutinized. Figure 2 shows the example for case #4. Here, a post-operative bleeding into the resection cavity was mistakenly segmented as viable tumour, giving rise to an apparent increase in tumour volume after surgery. The other segmented volumes (oedema, brain) remain plausible. This example confirms our choice of the pre-operative segmentation as a starting point for the model. The same reason applies to all three patients with apparently larger tumour after surgery.

Sensitivity analysis of cell migration velocity, receptor binding and λ_1

The influence of the most relevant undetermined model parameters, migration speed and receptor binding, is

Table 2
Variation of the parameters s, k^+ and assessment of the corresponding tumour simulation.

Tumour cell migration velocity s				
s [m/s]	1×10^{-6}	7.07×10^{-7}	2.5×10^{-7}	1×10^{-7}
s reduced to	100%	70.7%	25%	10%
Volume [cm^3]	980	731	255	134
Vol reduced to	100%	75%	26%	14%
	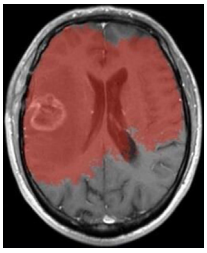	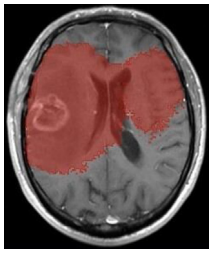	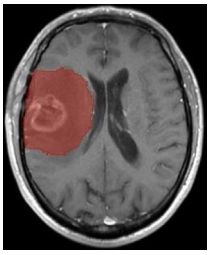	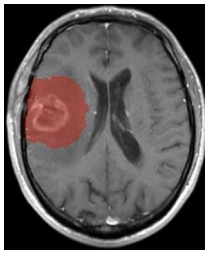
Receptor binding rate k^+				
k^+ [s^{-1}]	1.0		0.01	
k^+ reduced to	100%		1%	
Volume [cm^3]	899		853	
Vol reduced to	100%		94.9%	
	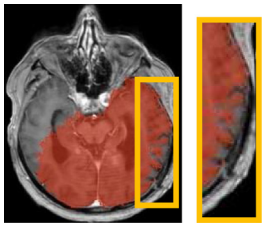		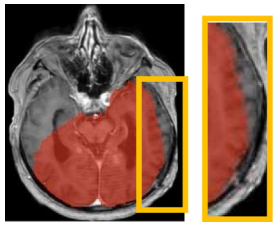	

displayed in Table 2 for an example patient. The main influence of the tumour migration speed is in the predicted tumour size. The receptor binding rate has little influence on the resulting tumour volume, but strongly determines the tumour shape, as it is the paramount parameter for isotropic or anisotropic migration along fibre tracts. Since the influence of λ_1 both on predicted tumour shape and volume was relatively weak, the best fit value of 0.01 s^{-1} was maintained for the following step.

Final model predictions

For the three patients with sufficient data for a complete modelling sequence, the results are presented in Table 3.

The future tumour evolution (day 103-212) could be predicted by the model with a dice coefficient better than 60% for all three patients. To achieve this amount of agreement, the cell migration speed s needed to be varied by a factor of 2.5, and the receptor attachment rate k^+ by a factor of 100. In all cases, the final tumour volume was overestimated by the model by a factor between 1.05 and 1.47.

Discussion and conclusions

Quality of model predictions

To evaluate the quality of the agreement between the model predictions and the ground truth, we must keep in mind that our gold standard relies on a single observer's (CB) manually-delineated tumour contours. We therefore decided to add a short validation of the stability and reliability of these contours by an inter-observer analysis including three other experienced radiation oncologists from our department (JF, JP, PM). As for the gold standard, they were asked to provide contours of the presumed clinical tumour extension based on the follow-up MRI images. The data sets were presented blinded as to the patient case and with no information on the model results or other physicians' contours, and the four contour sets were compared with each other and with the model predictions (Figure 3, Table 4).

In total, a dice coefficient between 63% and 89% is reached between the four different observers. While this falls short of the theoretically desirable value of 100%, a DCC of 70% or larger is generally considered as good agreement in the

Table 3
Comparison results and referenced simulation parameters for 3 patients.

Parameter	Patient a	Patient b	Patient c
Cell migration speed s [m/s]	$5.0 \cdot 10^{-7}$	$2.0 \cdot 10^{-7}$	$5.0 \cdot 10^{-7}$
Receptor binding rate k^+ [s^{-1}]	1.0	0.01	0.01
Grey scale/level set for final tumour delineation	1–255	50–255	1–255
Follow-up time [days]	119	103	212
Starting tumour volume [cm^3]	53.2	24.4	102.2
Predicted tumour volume [cm^3]	187.6	80.6	182.4
Gold standard [cm^3]	148.4	77.1	124.5
V(sim)/V(real)	1.26	1.05	1.47
DICE	0.66	0.62	0.65

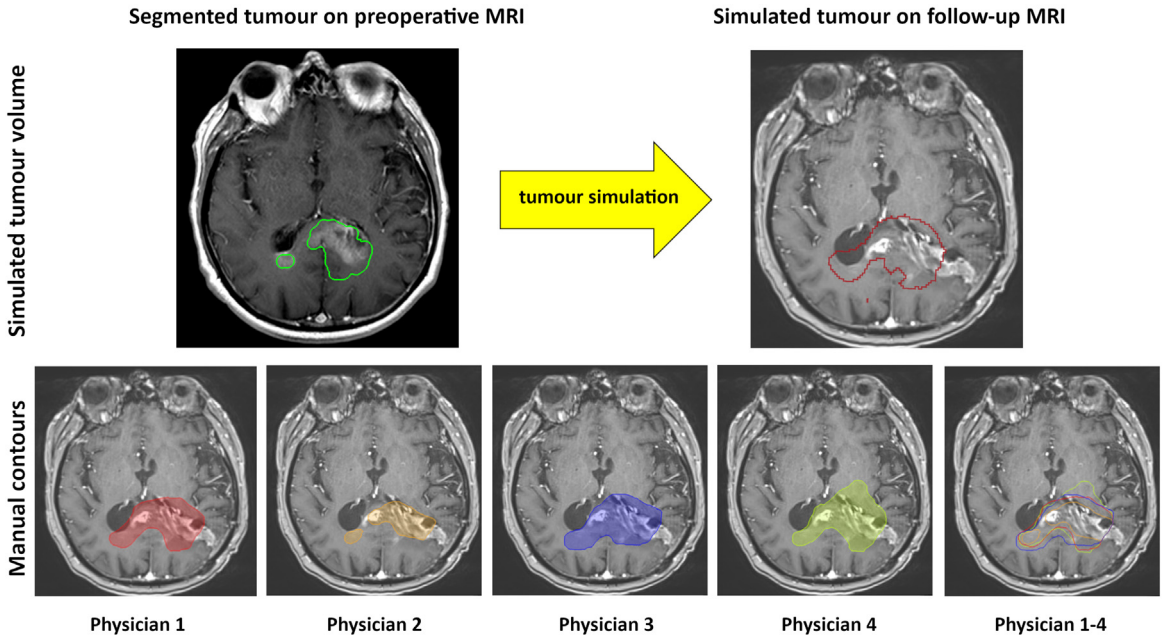

Figure 3. Upper panel: example of the preoperative segmentation and simulated future tumour extent for patient B. Lower panel: tumour delineations of four experienced physicians based on the real follow-up images of this patient.

Table 4
Differences in CTV-delineation between 4 experienced physicians. CTVs were contoured based on CT- and MRI data.

Inter observer analysis		Patient								
		A			B			C		
		DICE	Volume [cm^3]	V_{Phy}/V_R	DICE	Volume [cm^3]	V_{Phy}/V_R	DICE	Volume [cm^3]	V_{Phy}/V_R
Physician	1 (Reference)	–	148.3	–	–	64.2	–	–	124.5	–
	2	0.89	175.9	1.19	0.63	32.7	0.51	0.83	155.7	1.3
	3	0.89	168.9	1.14	0.76	93.6	1.46	0.85	120.9	0.97
	4	0.87	184.5	1.24	0.70	104.3	1.63	0.81	155.6	1.3

delineation of target volumes for radiotherapy [40,41]. Compared with this value, the model predictions (62–66%) perform reasonably well, keeping in mind the fact that these tumour volumes were created based on the pre-operative segmentation and DTI and extrapolated several months into the future by mathematical modelling.

Choice of the modelling approach

There are many available mathematical models for glioblastoma migration available in the present literature, which would warrant a similar study as performed here, and our model choice must remain arbitrary to some degree. A major

reason for our choice was the inclusion of the diffusion tensor imaging data. In some well-known approaches such as by Jbabdi et al. [42], the glioma diffusion direction is governed only by cell density and the magnitude of the diffusion coefficient is set constant for white and grey matter separately. We believe it is important to integrate the realistic directional distribution of white matter tracts, as glioblastoma cells are known to migrate preferentially along these. Therefore we opted for a model to integrate the DTI data so as to yield a more individualized migration behaviour for each patient and depending on the tumour origin. While this requires more input data, these are readily available, forming part of the routine pre-operative patient work-up. On the other hand, the inclusion of additional biological effects such as hypoxia as in [8], while increasing the realism in the model, requires information not generally available, calling for additional imaging such as positron-emission imaging which would entail additional radiation dose (and time for the patients). Still, there are a number of modelling approaches which could have been followed just as well as the model we chose [e.g., 11, 42], each with its own advantages and disadvantages.

Similarly, the choice which model parameters to keep fixed and which to vary in the optimization depended somewhat on the availability of literature information. In our particular case, R_0, k^- and λ_0 were taken from the literature [11,26,27,43], since at least some biological estimates for these parameters were available. Keeping these parameters constant, k^+, λ_1 and s were adjusted to achieve the best model fit, which was primarily intended to provide improved consistency with previous applications of our model. Clearly, the literature values are not precise, but rather estimates withing rather wide limits. For example, the total number of integrin receptors per cell (R_0) was estimated by [26] in the range $(2.1 \pm 0.2) \times 10^5$ for $\alpha V\beta 3$, $(2.3 \pm 0.2) \times 10^5$ for $\alpha 5\beta 1$, and $(1.6 \pm 0.2) \times 10^5$ for $\alpha V\beta 5$, which was simplified in the mathematical models by Engwer et al. [11] to 1×10^5. The turning rate λ_0 was taken from [43] as in previous modelling studies [10–12] as $0.1\ s^{-1}$. In fact, [43] observed a turning rate of between 60 and 80 degrees per 10 min for cells from a rat adenocarcinoma of the mammary gland, which may exhibit different behaviour than glioblastoma cells. Consequently, even those parameters fixed in our optimization may be tainted by inaccuracies. A different approach might have been to adjust all these parameters in the optimization procedure. From a practical perspective, this would have complicated the determination of the best fit, since the iterations were performed manually rather than using an automated cost function. Furthermore, different parameters can influence the model into similar directions, so that distinguishing the effects can become complex. Finally, only three patients were available for the final model evaluation. Adjusting all parameters may be achieved in the future using a large database of patients and machine-learning approaches to find patterns for the prediction of the tumour evolution.

In this study, we chose a pragmatic approach in which those parameters that could be estimated on biological grounds were kept constant and those that were undetermined were adjusted in the fit, so that the number of free parameters was kept to a minimum. In all modelling approaches, there is a trade-off in which a model with a larger number of free parameters will more easily provide a good fit to the data, at the risk of overfitting. Abiding by the principle of parsimony, the simplest explanation for the data should be preferred, which would be a "straightforward" model that would include all "real" effects without fitting superfluous fluctuations. Indeed, it would be interesting to perform a similar study comparing several models in terms of their performance, both from the point of view of different mathematical formulations and different numbers of free fit parameters. The adequacy of these models might then be compared using the Akaike information criterion or its refined versions, which weigh the accuracy of the model fit against the number of free parameters required to achieve this. However, this is beyond the scope of this study. The principle aim for this study consisted rather in proving the clinical feasibility and usefulness of such modelling approaches while exposing obstacles posed in the realistic setting, primarily the fact that the parameter values vary strongly and can only be determined with hindsight.

Clinical applicability

Although the model predictions are in reasonably good agreement with the realistic tumour growth, a major limitation for the clinical application arises from the fact that the optimum parameter choice varies over a large range. In particular, the optimum receptor attachment rate varies over two orders of magnitude for this small collective of only 3 patients. Even the smaller, 2,5-fold change in cell migration velocity would translate into a considerable change in predicted tumour volume. If optimum parameters for patient a were applied to patients b and c, the dice coefficients would drop to 36.8% and 47.4%, respectively. There is hence no "one-size-fits-all" parameter set which can be applied to predictive modelling at a stage before the first follow-up images are available. In the present study, the model parameters were determined by optimizing the parameters on the basis of the follow-up information. However, radiotherapy starts at the earliest possible time point after surgery, so predictive modelling must be performed at this time if it is to be of any use to radiotherapy planning. Only for a minority of patients will MRI information at various time points before surgical and adjuvant treatment be available, so that the parameters might be retrospectively fit to these data and the model predictions could be used for planning radio-oncologic treatment. However, for the vast majority of patients this information cannot be obtained when it is needed. Possibly in the future, in-vitro biological assays may provide a clue for the most important variables cell migration speed and receptor attachment rates, so that a realistic choice of model input parameters may become possible. Other multi-scale modelling approaches still leading to the same type of equations for the characterization of

tumour dynamics can require other parameters, depending on the respective description on the cell scale. For instance, the setting in [44] relies on a more detailed description of biomechanical effects influencing cell velocities, without involving any receptor binding and even relaxing the assumption of a constant cell speed. The brain tissue anisotropy (provided by DTI data) is captured in a similar way, while the only remaining parameter scales the cell acceleration, hence is related to cell motility. Whether such a (presumably patient-specific) parameter is easier to assess than a receptor binding rate is yet unclear, however at least its order of magnitude can probably be estimated from in-vitro assays (for further details refer to [44] and [8]).

If this major pitfall of parameter assessment could be resolved, the predictions for the model considered here and its variants/extensions accounting for further relevant features like tumour vascularization and hypoxia, necrosis etc. [6,8,9] might provide a reasonable basis for planning target definition in radiotherapy. Most tumour recurrences are observed in-field or at the field margins. If the density distribution of tumour cells inside the brain could be realistically predicted, regions with higher such densities might be treated with escalated dose concepts in a dose-painting approach. However, this will be for future studies to decide. At this point, mathematical models have made great progress in representing realistic cell behaviour including a wide spectrum of biological phenomena. Although our follow-up data was only sufficient for a detailed evaluation of three patients, these provide representative examples of the clinical reality. The model results were realistic and almost as good as the inter-observer variation in our sample. The prediction quality obtained therewith seems to be patient-dependent, which hints on patient-specific parameters. To our opinion, the next steps along the way towards realistic modelling must be the inclusion of biological information on the individual tumour properties of each patient, so that e.g. migration speed and behaviour in the presence of anisotropic tissue can be included in a personalized predictive model of tumour spread. A comprehensive diagnosis and therapy planning will ideally involve a team of biologists, radio-oncologists, neuro-radiologists and neurologists aided by mathematicians. With the advent of technology in cell biology, biomedical imaging, and computing power development such interdisciplinary approaches will increasingly get within reach.

Funding

Funded authors: A. Hunt, Ch. Engwer, M. Wenske, Ch. Surulescu.

Funding by the Federal Ministery for Education and Research in the GlioMaTh project 015M16UKB/PMA.

Declaration of interests

The authors declare no conflict of interest.

Acknowledgements

We are very thankful to an anonymous reviewer whose very constructive and precise comments have greatly improved this work.

References

[1] Optune. https://www.optune.com/hcp/instructions-for-use [accessed 20.11.20].
[2] Benson L. Tumor treating fields technology: alternating electric field therapy for the treatment of solid tumors. Sem Oncol Nurs 2018;34(2):137–50.
[3] Stupp R, Hegi ME, Mason WP, van den Bent MJ, Taphoorn MJB, Janzer RC, et al. Effects of radiotherapy with concomitant and adjuvant temozolomide versus radiotherapy alone on survival of glioblastoma in a randomised phase III study: 5-year analysis of the EORTC-NCIC trial. Lancet Oncol 2009;10:459–66.
[4] Stupp R, Taillibert S, Kanner A, Read W, Steinberg D, Lhermitte B, et al. Effect of tumor-treating fields plus maintenance temozolomide vs maintenance temozolomide alone on survival in patients with glioblastoma: a randomized clinical trial. JAMA 2017;318:2306–16.
[5] Angeli S, Emblem KE, Due-Tonnessen P, Stylianopoulos T. Towards patient-specific modelling of brain tumor growth and formation of secondary nodes guided by DTI-MRI. NeuroImage: Clin 2018;20:664–73.
[6] Conte M, Surulescu C. Mathematical modeling of glioma invasion: acid- and vasculature mediated go-or-grow dichotomy and the influence of tissue anisotropy; 2020 arXiv:2007.12204.
[7] Corbin G, Hunt A, Klar A, Schneider F, Surulescu C. Higher-order models for glioma invasion: from a two-scale description to effective equations for mass density and momentum Mathem. Models Methods Appl Sci 2018;28:1771–800.
[8] Corbin G, Engwer C, Klar A, Nieto J, Soler J, Surulescu C, et al. Modeling glioma invasion with anisotropy- and hypoxia-triggered motility enhancement: from subcellular dynamics to macroscopic PDEs with multiple taxis Mathem. Models Methods Appl Sci 2020, http://dx.doi.org/10.1142/S0218202521500056.
[9] Dietrich N, Kolbe N, Sfakianakis C, Surulescu. Multiscale modeling of glioma invasion: from receptor binding to flux-limited macroscopic PDEs; 2020 arXiv:2010.03277.
[10] Engwer C, Knappitsch M, Surulescu C. A multiscale model for glioma spread including cell-tissue interactions and proliferation. Math Biosci Eng 2016;13(2):443–60.
[11] Engwer C, Hunt A, Surulescu C. Effective equations for anisotropic glioma spread with proliferation: a multiscale approach and comparison with previous settings. Math Med Biol 2016;33:435–59.
[12] Engwer C, Hillen T, Knappitsch M, Surulescu C. Glioma follow white matter tracts: a multiscale DTI-based model. J Math Biol 2015;71:551–82.
[13] Hathout L, Patel V, Wen P. A 3-dimentional DTI MRI-based model of GBM growth and response to radiation therapy. Int J Oncol 2016;49:1081–7.
[14] Hatzikirou H, Basanta D, Simon M, Schaller K, Deutsch A. 'Go or Grow': the key to the emergence of invasion in tumour progression? Math Med Biol 2012;29:49–65.
[15] Hunt A, Surulescu C. A multiscale modeling approach to glioma invasion with therapy. Vietnam J Math 2016;45:221–40.
[16] Painter KJ, Hillen T. Mathematical modelling of glioma growth: the use of Diffusion Tensor Imaging (DTI) data to predict the anisotropic pathways of cancer invasion. J Theor Biol 2013;323:23–39.
[17] Saut O, Lagaert JB, Colin T, Fathallah-Shaykh HM. A multilayer grow-of-go model for GBM: effects of invasive cells and anti-angiogenesis on growth. Bull Math Biol 2014;76:2306–33.

[18] Scribner E, Fathallah-Shaykh HM. Single cell mathematical model successfully replicates key features of GBM: go-or-grow is not necessary. PLOS ONE 2017;12(1):e0169434.
[19] Jensen BM, Guldberg TL, Harbøll A, Lukacova S, Kallehauge JF. Diffusion tensor magnetic resonance imaging driven growth modelling for radiotherapy target definition in glioblastoma. Acta Oncol 2017;56(11):1639–43.
[20] Peeken JC, Molina-Romero M, Diehl C, Menze BH, Straube C, Meyer B, et al. Deep learning derived tumor infiltration maps for personalized target definition in Glioblastoma radiotherapy. Radiother Oncol 2019;138:166–72.
[21] Trip AK, Jensen MB, Kallehaute JF, Lukacova S. Individualizing the radiotherapy target volume for glioblastoma using DTI-MRI: a phase 0 study on coverage of recurrences. Acta Oncol 2019;58(10):1532–5.
[22] Unkelbach J, Menze BJ, Konukoglu E, Dittmann F, Le M, Ayache N, et al. Radiotherapy planning for glioblastoma based on a tumor growth model: improving target volume delineation. Phys Med Biol 2014;59(3):474–770.
[23] Witulla B, Goerig N, Putz F, Frey B, Engelhorn T, Dörfler A, et al. On PTV definition for glioblastoma based on fiber tracking of diffusion tensor imaging data; 2020.
[24] Uhm JH, Gladson CL, Rao JS. The role of integrins in the malignant phenotype of gliomas. Front Biosci: J Virtual Library 1999;4: D188–99.
[25] D'Abaco G, Kaye A. Integrins: molecular determinants of glioma invasion. J Clin Neurosci 2007;14:1041–8.
[26] Belkin AM, Tsurupa G, Zemskov E, Veklich Y, Weisel JW, Medved L. Transglutaminase-mediated oligomerization of the fibrin(ogen) αC domains promotes integrin-dependent cell adhesion and signaling. Blood J 2005;105:3561–8.
[27] Lauffenburger DA, Lindermann JJ. RECEPTORS models for binding, trafficking, and signaling. Oxford University Press; 1993.
[28] Diao W, Tong X, Yang C, Zhang F, Bao C, Chen H, et al. Behaviors of glioblastoma cells in in vitro microenvironments. Sci Rep 2019;9(1):1–9.
[29] Prag S, Lepekhin EA, Kolkova K, Hartmann-Petersen R, Kawa A, Walmod PS, et al. Ncam regulates cell motility. J Cell Sci 2002;115(2):283–92.
[30] Hunt A. DTI-based multiscale models for glioma invasion; 2017, published as: https://kluedo.ub.uni-kl.de/frontdoor/deliver/index/docId/5357/file/_DissertationAHunt_300DPI.pdf [accessed 26.08.20].
[31] Giese A, Westphal M. Glioma invasion in the central nervous system. Neurosurgery 1996;39:235–52.
[32] Bauer S, Fejes T, Meier R, Reyes M. BraTumIA a software tool for automatic brain tumor image analysis. Handbook 1.2; 2013.
[33] Porz N, Bauer S, Pica A, Schucht P, Beck J, Verma RK, et al. Multimodal glioblastoma segmentation: man versus machine. PLOS ONE 2014:e996873.
[34] Meier R, Knecht U, Loosli T, Bauer S, Slotboom J, Wiest R, et al. Clinical evaluation of a fully-automatic segmentation method for longitudinal brain tumor volumetry. Sci Rep 2016;6:23376.
[35] Kikinis R, Pieper SD, Vosburgh K. 3D Slicer: a platform for subject-specific image analysis, visualization, and clinical support; 2014.
[36] Dice L. Measures of the amount of ecologic association between species. Ecology 1945;26:297–302.
[37] Yoo TS, Ackerman MJ, Lorensen WE, Schroeder W, Chalana V, Aylward S, et al. Engineering and algorithm design for an image processing API: a technical report on ITK – the insight toolkit. In: Proc. of Medicine Meets Virtual Reality, J. Westwood, ed. IOS Press Amsterdam; 2002. p. 586–92.
[38] Cook PA, Bai Y, Nedjati-Gilani S, Seunarine KK, Hall MG, Parker GJ, et al.Camino: open-source diffusion-MRI reconstruction and processing, 14th scientific meeting of the international society for magnetic resonance in medicine. 2006. p. 2759.
[39] Aavatsmark I. An introduction to multipoint flux approximations for quadrilateral grids. Comput Geosci 2002;6:405–32.
[40] Vinod SK, Min M, Jameson MG, Holloway LC. A review of interventions to reduce inter-observer variability in volume delineation in radiation oncology. J Med Imaging Radiat Oncol 2016;60: 393–406.
[41] Kumar S, Holloway L, Roach D, Pogson E, Veera J, Batumalai V, et al. The impact of a radiologist-led workshop on MRI target volume delineation for radiotherapy. J Med Radiat Sci 2018;65:300–10.
[42] Jbabdi S, Mandonnet E, Duffau H, Capelle L, Swanson KR, Pélégrini-Issac M, et al. Simulation of anisotropic growth of low-grade gliomas using diffusion tensor imaging. Magn Reson Med 2005;54(3): 616–24.
[43] Sidani M, Wessels D, Mouneimne G, Ghosh M, Goswami S, Sarmiento C, et al. Cofilin determines the migration behavior and turning frequency of metastatic cancer cells. J Cell Biol 2007;179:777–91.
[44] Zhigun A, Surulescu C. A novel derivation of rigorous macroscopic limits from a micro-meso description of signal-triggered cell migration in fibrous environments; 2020 arXiv:2020.04148.